DOI - 10.68648/ijte-q-2026-49-03-003

Design Chart Development for Sustainable Sheet Pile Retaining Structures

Ramya L
M tech Student
Dept. of Civil Engineering
JNTUH University College of Engg. Sci. and Tech.
✉ ramyalaishetty599@gmail.com

Padmavathi M
Professor
Dept. of Civil Engineering
JNTUH University College of Engg. Sci. and Tech.
✉ mpadmace@jntuh.ac.in

ABSTRACT

Practical design tools for sheet pile wall applications are now necessary due to the growing need for affordable and sustainable retaining systems. For cantilever sheet pile walls under homogenous sand, homogeneous clay, and layered soil conditions, this study creates generalized non-dimensional equations and design charts. The suggested charts make it possible to quickly estimate the maximum bending moment and embedment depth, which eliminates the need for repeated analytical computations during early design. PLAXIS 3D finite element analysis and Rankine theory analysis were used to validate the analytical predictions, which showed good agreement and confirmed the dependability of the suggested method. Additionally, embodied carbon emissions were used to evaluate the environmental performance of standard steel sheet pile walls, recycled steel sheet pile walls, and reinforced concrete retaining walls. According to the findings, recycled steel sheet pile walls provide the best structural performance at the lowest carbon emissions. The created design charts encourage sustainable alternatives for earth-retaining structures and offer engineers a straightforward and effective design tool.

KEYWORDS *: Cantilever Sheet Pile Wall, Design Charts, Buckingham π Theorem, PLAXIS 3D, Sustainability.*

INTRODUCTION

The need for safe, affordable, and environmentally friendly retaining systems for excavations, basements, tunnels, waterfront buildings, and transit projects has grown due to the quick development of urban infrastructure. Because of its great strength, ease of installation, flexibility to adapt to various soil conditions, and possibility for reuse, steel sheet pile walls are utilized extensively. Because the immersed portion of the wall creates passive resistance, cantilever sheet pile walls are especially well suited for shallow to medium excavations. The preliminary design procedure is time-consuming since conventional analytical approaches require repeated calculations for different soil qualities and groundwater conditions, even if they offer dependable solutions for calculating embedment depth and maximum bending moment. Finite element analysis demands specialist software and a substantial amount of computational work, despite providing accurate prediction of soil-structure interaction. As a result, quick preliminary design is made possible by straightforward and dependable design tools. Furthermore, the significance of sustainable keeping systems with reduced embodied carbon emissions has been brought to light by growing environmental concerns. For cantilever sheet pile walls under homogenous sand, homogeneous clay, and layered soil conditions, this study creates generalized non-dimensional equations and useful design charts. PLAXIS 3D is used to validate the suggested analytical models, and embodied carbon assessment is used to analyze the sustainability of sheet pile walls made of reinforced concrete, conventional steel, and recycled steel. For the initial design of cantilever sheet pile retaining structures, the created design charts offer an effective and environmentally friendly method.

LITERATURE REVIEW

Sheet pile retaining wall design has advanced considerably through a combination of analytical, numerical, and reliability-based investigations.

Coulomb [1] and Rankine [2] first established the classical lateral earth pressure concepts that still underlie most retaining-structure analysis today. Terzaghi [3] brought soil mechanics principles into foundation engineering practice, and this was followed by Rowe [4] and Brinch Hansen [5], who worked out analytical procedures specifically for sheet pile wall design. Broms [6] later contributed further insight into how embedded retaining systems respond to lateral loading. Much of this design knowledge has since been formalized through manuals and codes, including NAVFAC [8], the U.S. Army Corps of Engineers [9], Eurocode 7 [25], and BS 8002 [27], along with established texts by Peck et al. [7], Bowles [11], Day [18], and Das [20], which together cover earth-pressure theory, embedment-depth calculation, and structural design of retaining systems across a range of soil conditions. Growth in computational geotechnics has since made it possible to model soil–structure interaction more accurately using finite element methods: Bilgin [22] applied numerical modelling to cantilever sheet pile wall behaviour, and Rajeev et al. [26] examined their seismic response through finite element analysis. Uncertainty in soil properties and loading has also been addressed through reliability-based frameworks, notably those of Ghazavi and Eslami [21] and of Ayyub and Ebeling [24]. Zakaria and Basha [28] more recently reviewed design methods for cantilever sheet pile walls in cohesionless soils and pointed to a continuing need for simplified procedures suited to everyday engineering practice. Despite this considerable body of analytical and numerical work, comparatively little effort has been directed toward generalized non-dimensional design charts spanning homogeneous sand, homogeneous clay, and layered soil conditions together, and the embodied-carbon performance of retaining systems has likewise received limited attention. This study addresses that gap by developing generalized non-dimensional equations and practical design charts for cantilever sheet pile walls, validating them against PLAXIS 3D results, and incorporating an embodied carbon assessment to support more sustainable retaining wall design.

METHODOLOGY

Design charts for anchored sheet pile walls are widely available in standard geotechnical references, but equivalent charts for cantilever sheet pile walls are limited, so their design typically relies on iterative analytical procedures. To address this gap, three representative soil profiles were adopted to capture the range of conditions commonly encountered in practice: (a) homogeneous sand, characterized by constant unit weight and angle of internal friction; (b) homogeneous clay, characterized by constant unit weight and undrained shear strength; and (c) a non-homogeneous, layered profile with sand above the dredge line and clay below it. Each profile was analysed with and without a groundwater table to capture the effect of hydrostatic pressure on wall behaviour.

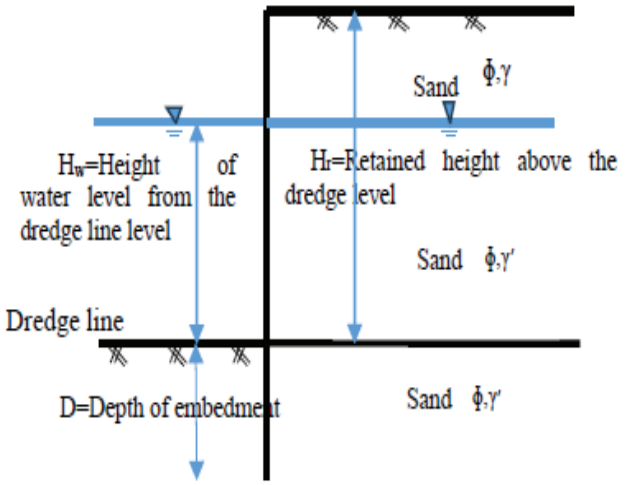


Fig. 1 Schematic cross-sections of the cantilever sheet pile wall embedded in (a) homogeneous sand

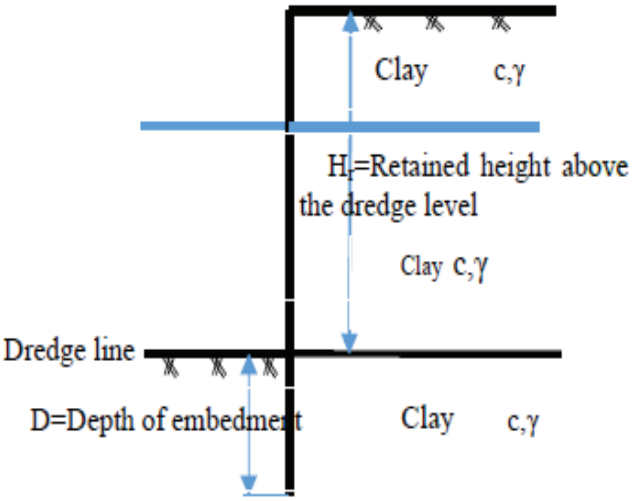


Fig.2 Schematic cross-sections of the cantilever sheet pile wall embedded in (b) homogeneous clay

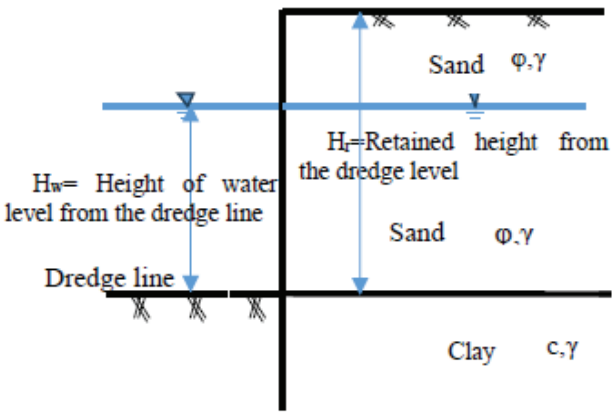


Fig.3 Schematic cross-sections of the cantilever sheet pile wall embedded in (c) layered soil

Rankine's earth-pressure theory, combined with the principle of limit equilibrium, forms the basis of the analytical formulation used here. For each soil profile, the active and passive lateral earth-pressure distributions were worked out along the wall depth and integrated to obtain the resultant forces together with their points of application.

Equilibrium of horizontal forces and of moments taken about the wall base was then applied to derive closed-form expressions for the required embedment depth (D) and the maximum bending moment (Mmax) acting on the wall. This framework provides the basis for the non-dimensionalization of the governing relationships that follows. The governing physical variables were reduced to a smaller set of independent dimensionless groups using the Buckingham π theorem, which allows the analytical results to be generalized across different soil and geometric conditions. For a phenomenon described by n governing variables involving m fundamental dimensions, it can be represented by Nπ independent dimensionless groups, Eq. (1):

$$N_{\pi} = n\text{-}m \quad (1)$$

For the homogeneous sand case, as illustrated in Fig. 1 the governing variables (D, Hr, Hw, γ, γ', φ) reduce, after non-dimensionalization, to the normalized embedment depth (D* = D/Hr), the groundwater ratio (H' = H_w/H_r), and the unit weight ratio (η = γ'/γ), as summarized

$$\pi_1 = \frac{D}{H_r} = D^*,\ \pi_2 = \frac{H_w}{H_r} = H',\ \pi_3 = \frac{\gamma'}{\gamma} = \eta$$

Several candidate functional forms linking these dimensionless groups were tested against the analytical results, and the coefficients giving the best fit were adopted, yielding the generalized design equations below. For homogeneous sand, the normalized embedment depth and normalized bending moment ($M^* = M/\gamma H r^3$) are given by Eq. (2) and (3):

$$\frac{D}{H_r} = [0.43 + 0.80(\mu^{0.20})] \times [1 + 0.32(H')(\eta^{0.20})] \quad (2)$$

$$\frac{M}{\gamma H_r^{\,3}} = \frac{0.15+0.108(\mu^{0.30})}{1+1.5H'} \quad (3)$$

Where, Hr=Retained height from the dredge level, Hw = Height of the water level from the dredge line, D/H_r = Normalized embedment depth =D^*, H_w/H_r = Groundwater level ratio =H', γ'/γ= Unit weight ratio = η, K_a / K_p = Ratio of earth coefficients = μ, $M/(\gamma H_r^3)$ = Normalized maximum bending moment =M^*

For homogeneous clay conditions shown in Fig. 2, the relevant dimensionless groups reduce to the unit weight ratio (η) and a cohesion-based stability parameter (λ = γHr/2c). The corresponding design equations for normalized embedment depth and normalized maximum bending moment are given by Eq. (4) and (5):

$$\frac{D}{H_r} = \frac{0.32\eta^{2.2}}{1+0.40\,\eta} \quad (4)$$

$$M_{max}/\gamma H_r^3 = 0.007\lambda^{2.4} / (1 + 0.75\lambda + 0.15\lambda^2) \quad (5)$$

Where, γ'/γ = Unit weight ratio=η, $(\gamma H_r)/2c$= Stability parameter for cohesive soils =λ

For the layered soil profile, as illustrated in Fig. 3 the additional cohesion parameter ($N_c = c/\gamma H_r$) and active earth-pressure coefficient (k_a) also enter the governing relationships. Eqs. (6) and (7) give the resulting normalized embedment depth and bending moment expressions for cases with a groundwater table, while Eqs. (8) and (9) give the equivalent expressions for dry conditions.

$$\frac{D}{H_r} = \frac{\left(0.74+0.25K_a^{0.5}\right)}{1+3(N_C)}\left(1+(H')(\eta)\right) \quad (6)$$

$$\frac{M}{\gamma H_r^{\,3}} = \frac{0.41\left(1+1.45K_a^{0.5}\right)}{1+4.4(N_C)} \quad (7)$$

$$\frac{D}{H_r} = \frac{1+0.65K_a{}^{0.5}}{1+3N_C} \quad (8)$$

$$\frac{M}{\gamma H_r{}^3} = \frac{0.41\left(1+1.45K_a{}^{0.5}\right)}{1+4.4(N_C)} \quad (9)$$

Corresponding equations without a groundwater table follow the same functional form with the H' term omitted, and separate coefficient sets were calibrated for each condition. The full set of non-dimensional equations for all three soil profiles, with and without groundwater, was used to generate the generalized design charts presented in the results.

The accuracy of the proposed methodology is then checked by comparing the analytical and numerical results through a percentage-error analysis. Alongside this, a sustainability assessment compares the embodied carbon emissions of reinforced concrete retaining walls, conventional steel sheet pile walls, and recycled steel sheet pile walls. Drawing on the analytical, numerical, and environmental findings together, the study closes with generalized conclusions and practical recommendations for economical, sustainable cantilever sheet pile wall design.

The total embodied carbon emissions are calculated as

$$EC = \sum_{i=1}^{n} (Q_i \times EF_i) \quad (10)$$

where

EC = Total embodied carbon emissions (kg CO_2 e)

Q_i = Quantity of the construction material

EF_i = Embodied carbon emission factor of the material (kg CO_2 e/unit)

n = Number of construction materials considered

Specifications

The soil properties used in this study were taken from standard geotechnical references and are representative of typical sand and clay deposits relevant to cantilever sheet pile wall design. The key geotechnical parameters considered are unit weight (γ), saturated unit weight (γ_{sat}), submerged unit weight (γ'), cohesion (c), angle of internal friction (ϕ), Young's modulus (E), Poisson's ratio (v), and the active earth pressure coefficient (K_a). In addition, the retained height (H_r), groundwater level (H_w), embedment depth (D), normalized embedment depth ($D^*=D/H_r$), maximum bending moment (M), normalized bending moment ($M^* = M/\gamma H_r^3$), active earth pressure coefficient (k_a), normalized cohesion parameter ($C/\gamma H_r$), and non-dimensional cohesion parameter ($N_c=\gamma H_r/2C$)were all fed into the analytical formulation and the Buckingham π theorem to derive the generalized non-dimensional equations and design charts. Together, these parameters control the active and passive earth pressures, embedment depth, bending moment, and overall stability of cantilever sheet pile walls. The same soil properties and parameters were used in both the analytical calculations and the PLAXIS 3D numerical models, which adopted the Mohr–Coulomb constitutive model to give a realistic representation of soil behaviour and a dependable basis for the generalized design equations and charts that follow.

PROPOSED FRAMEWORK

Figs. 1–3 illustrate the overall framework followed in this study. Work begins with a literature review used to pin down the research gap and objectives, followed by analytical investigations of homogeneous sand, homogeneous clay, and layered soil under both dry and groundwater conditions, applying Rankine and Coulomb earth-pressure theories. A parametric study then examines how the governing geotechnical parameters affect embedment depth, sheet pile length, and maximum bending moment for cantilever sheet pile walls.

The Buckingham π theorem is then used to derive generalized non-dimensional equations and matching design charts for the normalized embedment depth and normalized maximum bending moment. This methodology is checked against PLAXIS 3D finite element results, with the analytical and numerical outputs compared through a percentage-error analysis. The study concludes with a sustainability assessment comparing reinforced concrete, conventional steel, and recycled steel sheet pile walls, from which practical recommendations for sustainable cantilever sheet pile wall design are drawn.

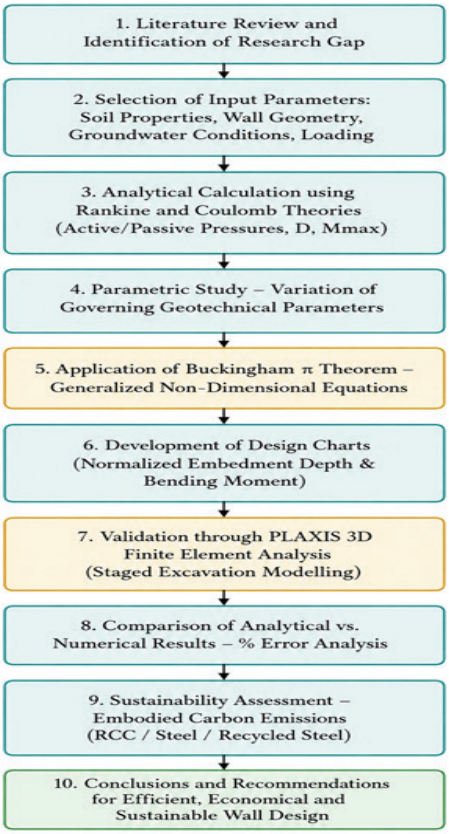


Fig. 4 Proposed framework flow chart

RESULTS AND DISCUSSION

Validation of Analytical Predictions using PLAXIS 3D

Validation of the proposed non-dimensional equations and design charts was carried out using three-dimensional finite element analysis in PLAXIS 3D, with numerical simulations run for selected cases of homogeneous sand, homogeneous clay, and layered soil, using the same soil parameters, sheet pile properties, and groundwater conditions as the analytical study. Soil behaviour was represented using the Mohr–Coulomb model, and the sheet pile wall itself was modelled with plate elements assigned appropriate structural properties.

Table 1 summarizes the comparison between the numerical and analytical values of embedment depth and maximum bending moment, along with the percentage error used to gauge the accuracy of the developed relationships. Analytical and numerical solutions agreed well overall, with errors averaging roughly 5–14% across the cases examined, which supports the reliability of the proposed design charts for cantilever sheet pile walls across the soil and water-table conditions considered. On this basis, the generalized design charts presented in the following subsections can be applied with reasonable confidence.

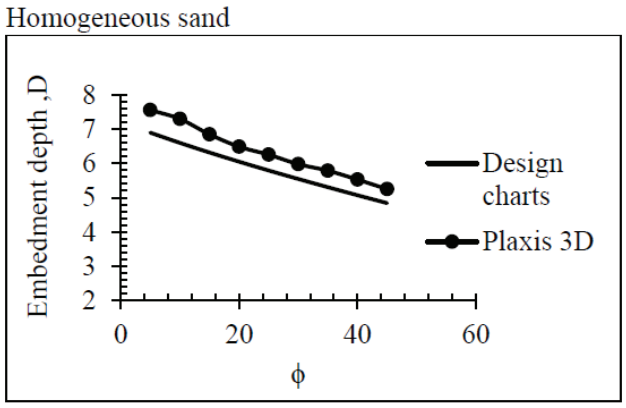


Fig. 5 Comparison of Design Charts and PLAXIS 3D Results for D vs ϕ

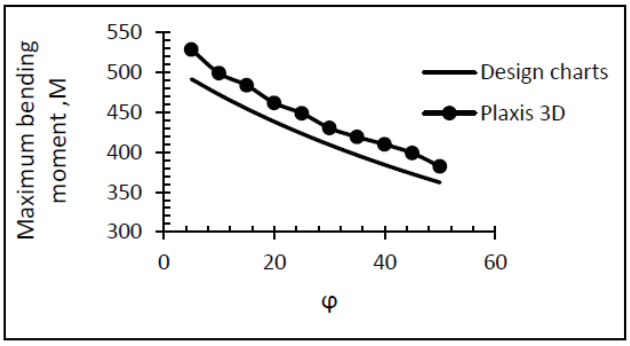


Fig. 6 Comparison of Design Charts and PLAXIS 3D Results for M vs ϕ

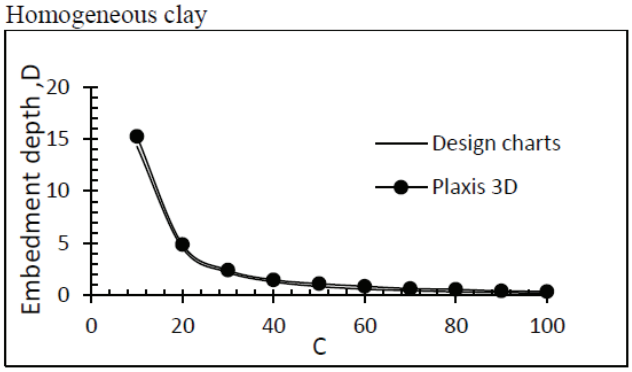


Fig. 7 Comparison of Design Charts and PLAXIS 3D Results for D vs Cohesion

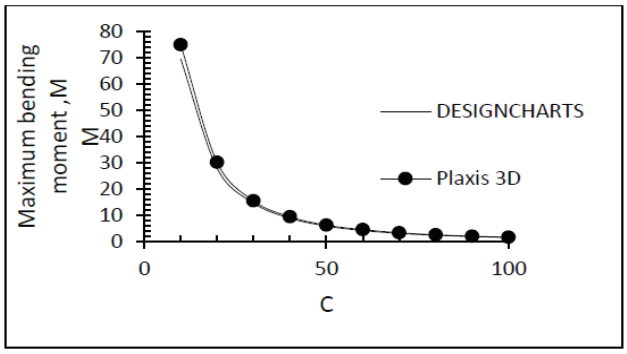


Fig. 8 Comparison of Design Charts and PLAXIS 3D Results for M vs Cohesion

Layered soil

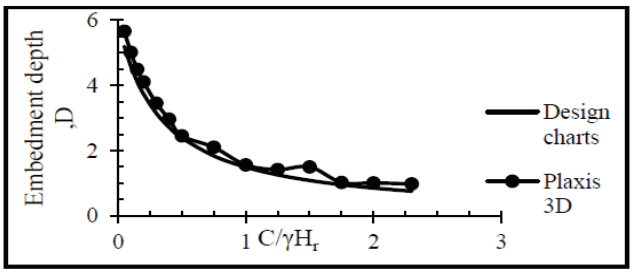


Fig. 9 Comparison of Design Chart and PLAXIS 3D Results for c/(γH$_r$)vs. D under Groundwater Conditions

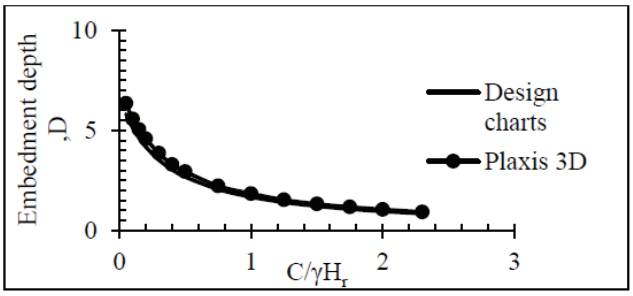


Fig. 10 Comparison of Design Chart and PLAXIS 3D Results for c/(γH$_r$)vs. D*under Dry Conditions

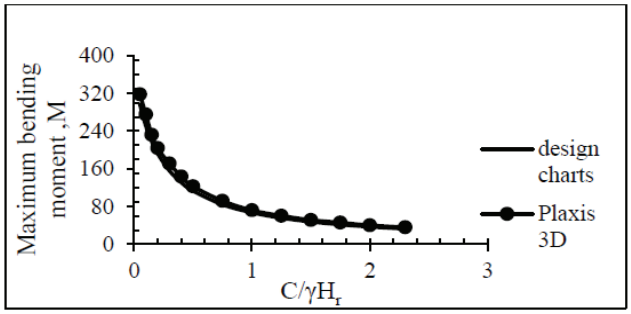


Fig. 11 Comparison of Design Charts and PLAXIS 3D Results for c/(γH$_r$) vs M under Groundwater Conditions

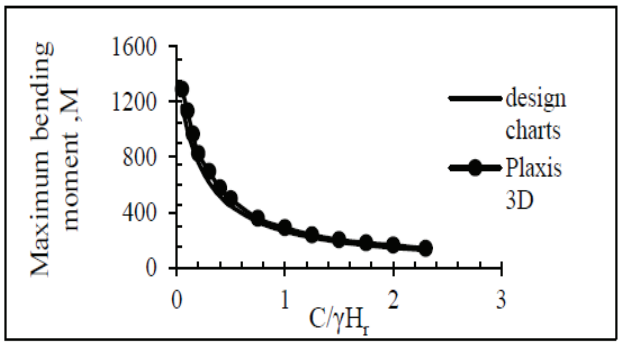


Fig. 12 Comparison of Design Charts and PLAXIS 3D Results for c/(γH$_r$) vs M under Groundwater Conditions

Table 1. Comparison of design-chart predictions with PLAXIS 3D simulations

Case	Comparison	Average Error (%)	Error Range (%)
Homogeneous sand	Embedment depth (D) vs φ	8.68	7.25 – 10.59
Homogeneous sand	Bending moment (M) vs φ	6.11	5.12 – 7.52
Homogeneous clay	Bending moment (M) vs cohesion	7.22	5.86 – 9.11
Homogeneous clay	Embedment depth (D) vs cohesion	9.34	6.30 – 13.04
Layered soil (with water table)	D vs c/γHr	10.40	2.51 – 27.62
Layered soil (without water table)	D vs c/γHr	9.04	8.06 – 9.98
Layered soil (with water table)	M vs c/γHr	8.47	5.80 – 10.18
Layered soil (without water table)	M vs c/γHr	9.91	7.13 – 13.95

The proposed non-dimensional design charts are validated in Figures 5–12, which set the analytical predictions against PLAXIS 3D results for three representative cases: homogeneous sand (Figs. 5–6), homogeneous clay (Figs. 7–8), and layered soil, sand over clay, examined both with (Figs. 9–10) and without (Figs. 11–12) a groundwater table. Table 1 shows the average prediction error falling between 6.11%

and 10.40%, with most cases below 10%, indicating close agreement between the analytical and PLAXIS 3D solutions. This confirms that the proposed non-dimensional equations and design charts can reliably estimate embedment depth and maximum bending moment for cantilever sheet pile walls across the soil and groundwater conditions studied.

Design Charts for Cantilever Sheet Pile Walls

Using the Buckingham π theorem, generalized non-dimensional equations were derived for cantilever sheet pile walls in homogeneous sand, converting the analytical results into dimensionless relationships for the normalized embedment depth (D/H) and normalized maximum bending moment (Mmax/γHr

These non-dimensional equations were then used to build practical design charts for homogeneous sand, allowing the normalized embedment depth and normalized maximum bending moment to be estimated quickly without repeating the analytical calculations each time.

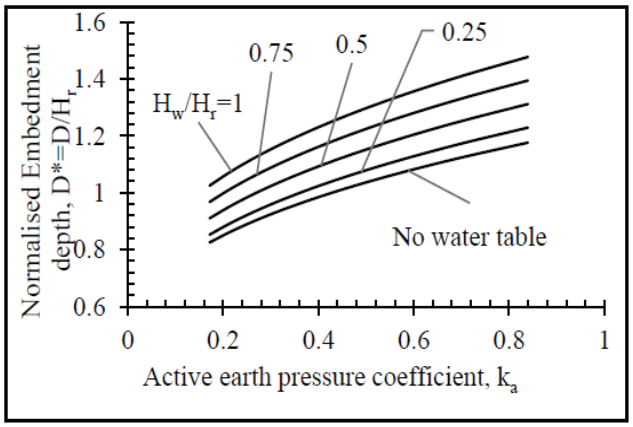


Fig. 13 Variation of normalized embedment depth, D* with active earth pressure coefficient, k_a

Figure 13 presents the design chart relating normalized embedment depth (D/H_r) to the active earth pressure coefficient (K_a) under varying groundwater conditions, based on the proposed relationship given in Eq. (2). As K_a increases from 0.2 to 0.8, D/H_r rises by roughly 50%, and a higher groundwater level pushes the required embedment depth up further, by around 20–25%. This chart therefore serves as a quick design tool for cantilever sheet pile walls across different groundwater conditions.

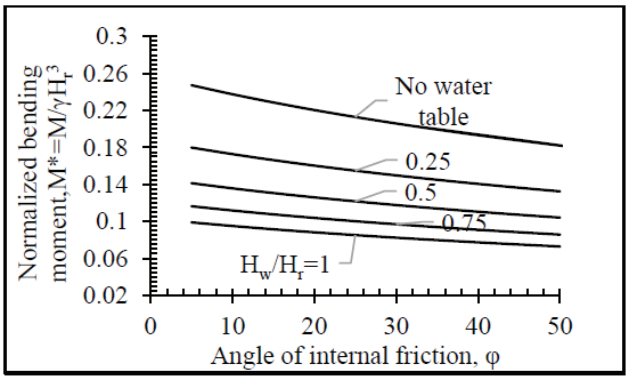


Fig. 14 Variation of normalized bending moment, M^* with angle of internal friction angle, φ

Figure 14 presents the design chart relating the normalized bending moment (M^*) to the angle of internal friction (ϕ), developed using the non-dimensional relationship given in Eq. (3). As ϕ increases from 5° to 50°, the normalized bending moment decreases by approximately 60–70%, while increasing the groundwater ratio (H_w/H_r)from 0 to 1.0 further reduces M^* by around 55–65%. This makes the chart a fast and dependable means of estimating the normalized bending moment of cantilever sheet pile walls under varying groundwater conditions.

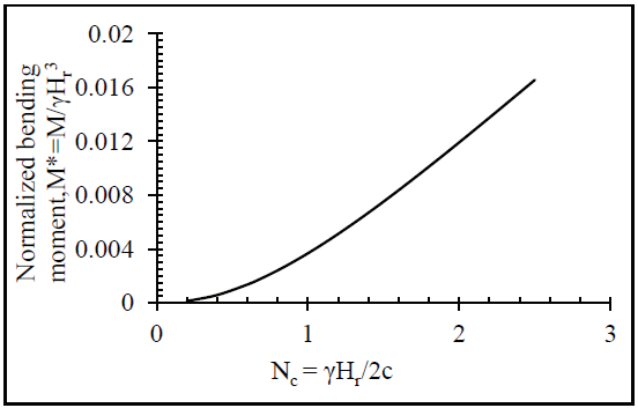


Fig. 15 Variation of the normalized bending moment, M^* with the soil strength parameter, $N_c = (\gamma H_r)/2c$

Figure 15 presents the variation of normalized bending moment ($M^* = M/\gamma H_r^3$) with the non-dimensional cohesion parameter ($N_c = \gamma H_r/2C$) for homogeneous clay under dry conditions, based on the proposed relationship given in Eq. (4). The chart shows that M^* increases with increasing N_c, indicating reduced cohesion influence and higher bending demand. For

example, M^* increases from approximately 0.008 at N_c = 1.5 to 0.016 at N_c = 2.5. The developed design chart provides a simple approach for estimating bending moments in cantilever sheet pile walls.

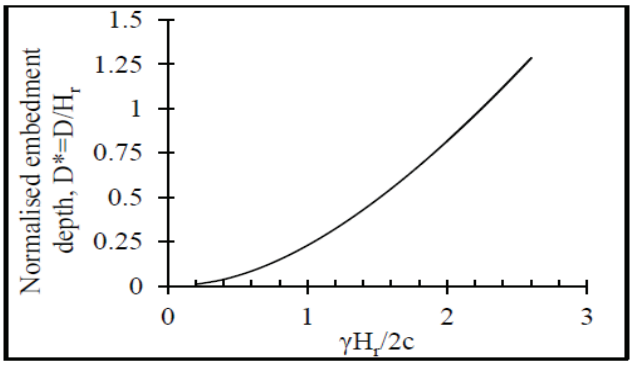


Fig. 16 Variation of the normalized depth ratio D* with the normalized soil parameter (γH_r)/2c

Figure 16 presents the variation of normalized embedment depth ($D^* = D/H_r$)with the non-dimensional cohesion parameter ($N_c = \gamma H_r/2C$)for homogeneous clay under dry conditions, based on Eq. (5). The results show that D^*increases with N_c, rising from approximately 0.50 at N_c = 1.5 to 1.30 at N_c =2.6, reflecting the greater embedment needed as the influence of cohesion diminishes. The proposed chart offers a dependable way of estimating embedment depth for cantilever sheet pile walls.

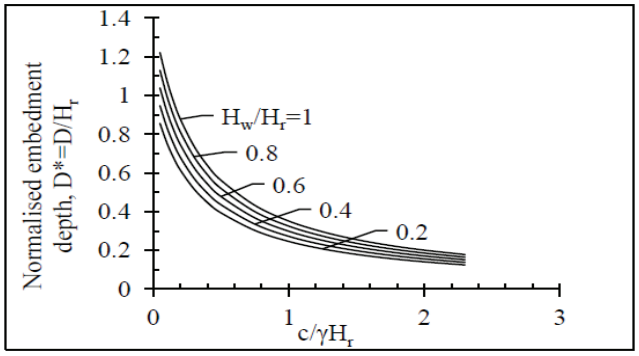


Fig. 17 Variation of the normalized cohesion parameter with the normalized depth ratio D* in the absence of water table

Figure 17 presents the variation of normalized embedment depth ($D^* = D/H_r$) with the normalized cohesion parameter ($C/\gamma H_r$) for non-homogeneous soil under different groundwater levels, based on the relationship given in Eq. (6). The results show that D^* decreases with increasing cohesion, whereas higher groundwater levels increase the embedment requirement. At $C/\gamma H_r$ = 1.0, D^* increases from 0.22 to 0.35 as H_w/H_{rrises} from 0.2 to 1.0. This design chart offers an efficient means of estimating embedment depth for cantilever sheet pile walls under varying groundwater conditions.

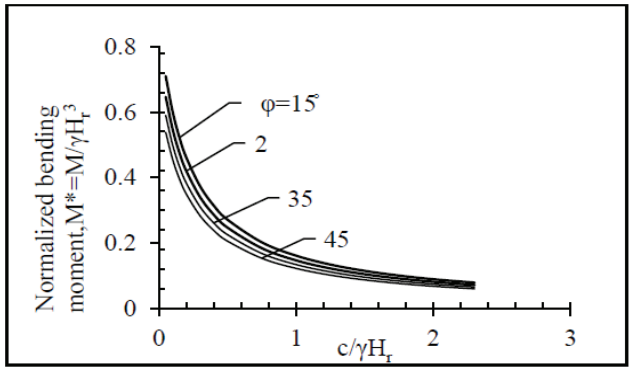


Fig. 18 Variation of the normalized cohesion parameter c/(γH_r) with the non-dimensional moment parameter, M* in the absence of water table

Figure18 presents the variation of normalized bending moment ($M^* = M/\gamma H_r^3$)with the normalized cohesion parameter($C/\gamma H_r$) for non-homogeneous soil at different friction angles without groundwater, following the relationship in Eq. (7). The results indicate that M^* decreases with increasing cohesion and friction angle due to enhanced soil strength and reduced lateral earth pressure. At $C/\gamma H_r$ = 1.0, M^* decreases from 0.17 to 0.11 as ϕ rises from 15° to 45°. The chart therefore gives a dependable tool for estimating bending moments in cantilever sheet pile walls under dry conditions.

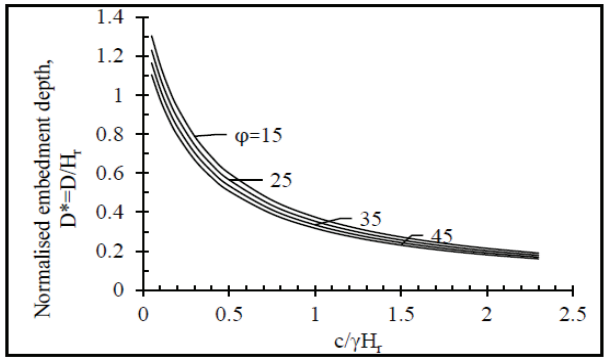


Fig. 19 Variation of the normalized cohesion parameter c/(γH_r)with the normalized depth ratio D* in the presence of water table

Figure 19 presents the variation of normalized embedment depth ($D^* = D/H_r$)with the normalized cohesion parameter ($C/\gamma H_r$) for non-homogeneous soil at different friction angles with groundwater present, following the relationship in Eq. (8). The results show that D^* decreases with increasing cohesion and friction angle due to enhanced soil resistance. At $C/\gamma H_r = 1.0$, D^* reduces from 0.35 to 0.29 as ϕ increases from 15° to 45°. The proposed chart provides a reliable approach for estimating embedment depth of cantilever sheet pile walls.

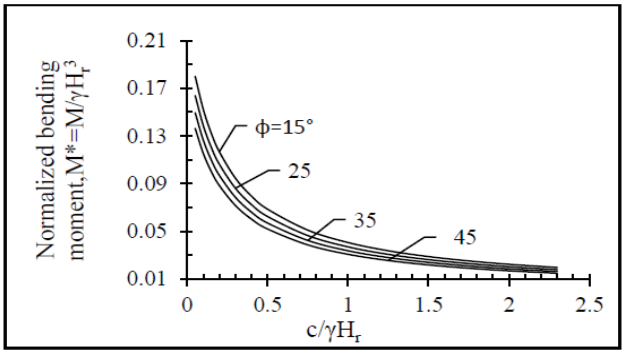


Fig. 20 Variation of the normalized cohesion parameter c/(γH$_r$) with the non-dimensional moment parameter M* in the presence of water table

Figure 20 presents the variation of normalized bending moment ($M^* = M/\gamma H_r^3$)with the normalized cohesion parameter ($C/\gamma H_r$) for non-homogeneous soil at different friction angles with groundwater present, following the relationship in Eq. (9). The results show that M^* decreases with increasing cohesion and friction angle due to reduced lateral earth pressure. At $C/\gamma H_r = 1.0$, M^* reduces from 0.038 to 0.029 as ϕincreases from 15° to 45°. The proposed chart provides a reliable approach for estimating bending moments of cantilever sheet pile walls.

Figure 21 sets out the CO_2 emissions of the three retaining wall systems for a 1 m wall length. The RCC retaining wall generates the most emissions (3765 kg CO_2-e), the conventional steel sheet pile wall comes next (2736 kg CO_2-e), and the recycled steel sheet pile wall produces the least (864 kg CO_2-e). Switching to recycled steel therefore cuts CO_2 emissions by around 68% relative to conventional steel and by 77% relative to the RCC wall, underlining its stronger environmental performance.

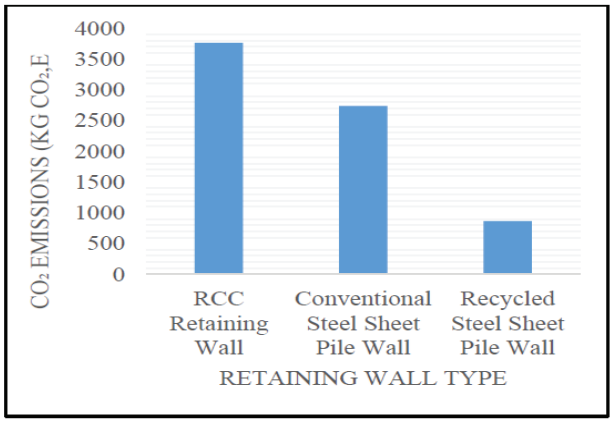


Fig. 21 Comparison of CO_2 Emissions of Different Retaining Wall Systems

CONCLUSIONS

The design charts for homogeneous sand showed that the normalized embedment depth increased from 0.82 to 1.48 with an increase in K_a from 0.2 to 0.8, while the normalized bending moment fell by 25–30% as the friction angle increased. Both parameters rose under groundwater conditions because of hydrostatic pressure effects. For homogeneous clay, the parameter $N_c = \gamma H_r/2c$ significantly influenced wall behaviour, with an increase in N_c rising from 0.25 to 2.5 pushed the normalized embedment depth up from 0.02 to 1.28 and the bending moment from 0.0002 to 0.016. The layered soil design charts successfully captured the effects of soil stratification and groundwater conditions. Increasing $c/\gamma H_r$ brought down both the normalized embedment depth and bending moment, while the presence of groundwater increased the wall's response. PLAXIS 3D simulations validated the proposed analytical equations, with errors ranging from 7.1% to 14.0% and averaging around 10%, supporting the reliability of the methodology developed. The sustainability assessment further showed that recycled steel sheet piles cut embodied carbon emissions by 68% relative to conventional steel sheet piles and by 77% relative to RCC retaining walls, pointing to their potential as a more sustainable retaining option.

ACKNOWLEDGEMENT

The authors gratefully thank Dr. M. Padmavathi, Professor, Department of Civil Engineering, University College of Engineering Science & Technology

Hyderabad (UCESTH), JNTUH, for her guidance, encouragement, and constructive input throughout this work. The authors also thank UCESTH, JNTUH, for the academic facilities and support extended during the course of this study.

REFERENCES

1. C. A. Coulomb, "Essay on the Application of the Rules of Maxima and Minima to Some Problems of Statics Related to Architecture," Memoirs of the Royal Academy of Sciences, Paris, France, 1776.
2. W. J. M. Rankine, "On the Stability of Loose Earth," Philosophical Transactions of the Royal Society of London, vol. 147, pp. 9–27, 1857.
3. K. Terzaghi, Theoretical Soil Mechanics. New York, NY, USA: John Wiley & Sons, 1943.
4. P. W. Rowe, "Anchored Sheet-Pile Walls," Proceedings of the Institution of Civil Engineers, vol. 1, no. 1, pp. 27–70, 1952.
5. J. Brinch Hansen, "Earth Pressure Calculation," The Danish Geotechnical Institute Bulletin, Copenhagen, Denmark, 1953.
6. B. B. Broms, "Lateral Resistance of Piles in Cohesive Soils," Journal of the Soil Mechanics and Foundations Division, ASCE, vol. 90, no. SM2, pp. 27–63, 1964.
7. R. B. Peck, W. E. Hanson, and T. H. Thornburn, Foundation Engineering, 2nd ed. New York, NY, USA: John Wiley & Sons, 1974.
8. U.S. Department of the Navy, Foundations and Earth Structures, NAVFAC Design Manual DM 7.02. Alexandria, VA, USA: Naval Facilities Engineering Command, 1986.
9. U.S. Army Corps of Engineers, Engineering Manual EM 1110-2-2504: Design of Sheet Pile Walls. Washington, DC, USA: Department of the Army, 1994.
10. U.S. Army Corps of Engineers, Engineering and Design—Design of Sheet Pile Walls, EM 1110-2-2504, Washington, DC, USA: Department of the Army, Jul. 1994.
11. J. E. Bowles, Foundation Analysis and Design, 5th ed. New York, NY, USA: McGraw-Hill, 1996.
12. Naval Facilities Engineering Command (NAVFAC), Foundations and Earth Structures, Design Manual DM-7.02, Alexandria, VA, USA: NAVFAC, 1986.
13. Bureau of Indian Standards, IS 14458 (Part 1): 1998—Guidelines for Retaining Wall for Hill Areas: Selection of Type of Wall. New Delhi, India: BIS, 1998.
14. Bureau of Indian Standards, IS 14458 (Part 2): 1997—Guidelines for Retaining Wall for Hill Areas: Design of Retaining/Breast Walls. New Delhi, India: BIS, 1997.
15. Bureau of Indian Standards, IS 14458 (Part 3): 1998—Guidelines for Retaining Wall for Hill Areas: Construction of Dry Stone Walls. New Delhi, India: BIS, 1998.
16. Bureau of Indian Standards, IS 14458 (Part 4): 1998—Guidelines for Retaining Wall for Hill Areas: Construction of Retaining and Breast Walls. New Delhi, India: BIS, 1998
17. W. Powrie, Soil Mechanics: Concepts and Applications. London, U.K.: E & FN Spon, 1996.
18. R. W. Day, Geotechnical and Foundation Engineering: Design and Construction. New York, NY, USA: McGraw-Hill, 1999.
19. R. W. Day, Foundation Engineering Handbook: Design and Construction with the 2001 International Building Code. New York, NY, USA: McGraw-Hill, 2001.
20. B. M. Das, Principles of Foundation Engineering, 6th ed. Belmont, CA, USA: Thomson Brooks/Cole, 2007.
21. M. Ghazavi and A. Eslami, "Reliability-Based Design of Cantilever Sheet Pile Walls in Sandy Soils," International Journal of Civil Engineering, vol. 6, no. 4, pp. 257–268, 2008.
22. Ö. Bilgin, "Numerical Studies of Cantilever Sheet Pile Walls," Computers and Geotechnics, vol. 37, no. 3, pp. 399–407, 2010.
23. D. P. Coduto, M. R. Yeung, and W. A. Kitch, Geotechnical Engineering: Principles and Practices, 2nd ed. Upper Saddle River, NJ, USA: Pearson, 2011.
24. B. M. Ayyub and R. M. Ebeling, Reliability-Based Design of Sheet Pile Structures. Reston, VA, USA: ASCE Press, 2011.
25. British Standards Institution, BS EN 1997-1:2004+A1:2013 Eurocode 7: Geotechnical Design—Part 1: General Rules. London, U.K.: BSI, 2013
26. P. Rajeev, Q. Bui, and N. Sivakugan, "Seismic Behaviour of Sheet Pile Retaining Walls Using Finite Element Analysis," Soil Dynamics and Earthquake Engineering, vol. 75, pp. 115–126, 2015.
27. British Standards Institution, BS 8002:2015—Code of Practice for Earth Retaining Structures. London, U.K.: BSI, 2015.
28. M. Zakaria and M. Basha, "A Review on Cantilever Sheet Pile Wall Design in Cohesionless Soils," Journal of Geotechnical and Geoenvironmental Engineering, vol. 150, no. 2, 2024.